Carbon Trends 17 (2024) 100412

Contents lists available at ScienceDirect

Carbon Trends

journal homepage: www.elsevier.com/locate/cartre

Optical investigation of degradation of graphene oxide in alkaline environment: Evidence of two distinct photon-emitting phases in visible region.

Emiliano Burresi [a,*], Maria Lucia Protopapa [b]

[a] ENEA, SSPT-TIMAS-CMS, Brindisi Research Center, S.S. 7 Appia km 706, 72100, Brindisi, Italy
[b] ENEA, SSPT-EC-RMP, Brindisi Research Center, S.S. 7 Appia km 706, 72100, Brindisi, Italy

ARTICLE INFO

Keywords:
Oxidative debris
Graphene oxide
Carbon quantum dots
Reduction
Deoxygenation

ABSTRACT

In this work we show a procedure of treating of the graphene oxide in alkaline environment as a function of the treatment time in order to obtain novel structures with strong luminescence properties, water-stable, useful as potential replacement for critical raw materials employed as example in optical and optoelectronic devices or for diagnostic and therapeutic technology. These structures have distinct blue and green-luminescence properties which derived most likely from different structural conformations, one associable with that of carbon quantum dots (or as an alternative to that of the Oxidative Debris), the other, lighter and more similar to organic compounds, reported in literature as fulvic-like molecules, but whose nature has to be further investigated. We show that the lighter fraction has a dual mechanism of photoemission: the excitation-independent PL for excitation wavelength within 350 nm and the excitation-dependent component for excitation wavelength ranging in the visible spectrum. The PL dual behaviour could depend on fluorescent nanoclusters composed by specific organic fluorophores with a carbonaceous core. FTIR analysis shows reasonably the same functional groups unless of some difference discussed in the text, meanwhile UV–Vis and PL analysis clearly highlight two distinct emissions (450 nm and 530 nm) in the visible region of the electromagnetic spectrum. Excitation-dependent photoluminescence, water stability and organic fluorescent nanostructures are issues particularly required for application in the biological field but also in materials science.

1. Introduction

In recent few decades much research in science and technology has required enormous efforts to keep up with the changes in our society towards a more sustainable future regarding intense human activities such as the production of goods and services and an increasing attention to the impact on the environment and territorial systems [1]. In fact, it is well known that in recent years the increase of the demand for development of clean technologies which are not dependent on fossil fuels has become relevant and much attention has been focused about the use of critical materials [2-3] and their substitution. Moreover, the development of devices free of critical raw materials has become crucial for technologies such as light emitting diode, PV, batteries, and in general electronic and optoelectronic devices. Carbon based materials can have a strategic role for the development of these technologies for their peculiar properties such as electronic conductivity (graphite, graphene, reduced graphene oxide, carbon nanotubes) [4-8] together with optical and optoelectronic ones (carbon dots, graphene oxide and graphene quantum dots) [9-13] as well as for applications in additive manufacturing (3D printing) [14]. Carbon-based materials are very light materials, low cost and easy to recover and recycle. Moreover, novel fluorescent materials with high biocompatibility, tuneable emission and stability in water are highly studied as game-changer materials to overcome the current ones employed in diagnostic and therapeutic applications.

In this framework of applications, recently a review about alkaline treatment of graphene oxide has been published [15]. In this work, the authors summarize ten years of research about the alkaline treatment of graphene oxide, useful to obtain as example a material with good conductivity (σ= 1–10 S m^{-1}), which is comparable to the conductivity of some reduced GO obtained through more traditional routes [16]. By following this reference [15] the effect of this alkaline washing is the

* Corresponding author.
E-mail address: emiliano.burresi@enea.it (E. Burresi).

https://doi.org/10.1016/j.cartre.2024.100412
Received 4 April 2024; Received in revised form 26 September 2024; Accepted 6 October 2024
Available online 9 October 2024

formation of special structures named Oxidative Debris (ODs) which are structures already present on the surface of GO [17-19], made of highly oxidized polyaromatic fragments, and generated by strong oxidation of graphite by means of typical synthesis such as Hummers, Brodie and Staudenmaier methods [20-22]. Similar structures have been found on the surface of carbon nanotubes and isolated after purification [23]. From the earliest papers on ODs [24], the authors highlighted the significance of these carboxylated carbonaceous fragments in determining the surface properties of graphene oxide. Surprisingly, despite their importance, some reviews in the field [25-26] have not mentioned ODs.

Regarding ODs earliest papers, the paper by Rourke et al. [16] is generally taken as seminal reference. Previously, the excellent review [27] on the properties and applications of GO and reduced GO did not mention anyway the presence of ODs on the GO surface, although alkaline treatment as a method of reducing GO was mentioned in this review [28], previous to the Rourke's paper. In recent times, the authors of the cited reference [15] stated again the importance of the role of the ODs on several properties of GO (optical, electrochemical, antimicrobial, mechanical and so on) underlining once again as several authors completely neglect the existence of ODs in GO [29-30]. In fact, restricting to the past three years the research on graphene oxide reviews, we found many manuscripts on GO that do not cite the role of the ODs [31-53], although all these references are only a partial list of all publications on the GO in the last three years. They regard many applications of the GO in several technological fields such as materials in nanomedicines and biomedicine [31,33], for catalysis and photocatalysis [34,35], sensing [36,37], antimicrobial [38], energy storage and capacity [39,40], photonic [41], optoelectronic [42,43], memory [44], pollutant [45], water purification [46] and more generally material for composites and polymeric filler [47,48]. Many of these applications need pristine carbon sp^2 structure that have oxygen moieties bonded on the sp^2 plane in order to convert it in a semiconductor material with finite band-gap, as well as better stability in hydrophilic environment, improving also its biocompatibility. Moreover, the reduction processes of GO to obtain reduced GO reported in this paper list involves different types of techniques which are the traditional routes for reduction of GO such as chemical reduction with hydrated hydrazine, hydride, $NaBH_4$, hydroquinone, ascorbic acid, thermal treatment in inert and reductive environment (usually Ar/H_2) at high temperature (above 200 °C) other than electrochemistry and photocatalytic reduction by using ultraviolet (UV) radiation. Among all these reduction techniques, the only process suspected to produce ODs is the alkaline treatment in NaOH o KOH that for some authors is attributable to the base-washing [15] which should break the π-π and Wan der Waals interaction separating the most superficial oxidized phase from the basal plane of the graphene oxide.

Furthermore, restricting the bibliographical research of the regular articles published on 2024 having GO as topic (using as search string the words graphene oxide in title, keywords and abstract) only a very restricted number of these articles contains also the oxidative debris words [54-60]. Hence, from this brief bibliographical dissertation only a small part of the scientific literature attributes to the ODs the properties of the graphene oxide and they are mentioned mainly in the case of alkaline treatments of GO. However, it is surely true that the base-washing produces carbonaceous fragments strongly oxidized which can be treated as an independent material and potentially engineerable.

As reported in [15] the deep meaning of the ODs can be rather different, but reasonably these objects are generally identified like structures 2–10 nm in size (but in literature size about 50 nm are also reported [15]), heavily oxidized with a C/O ratio lower than 1, against a C/O ratio for pristine GO (also named aGO) ranging from 0.8 to 2.3. For base-washed GO (bwGO) C/O is reported about 4.5, even though these values have an undetectable variability, and it is not unlikely that some authors found C/O ratio very similar for both aGO and bwGO. In our recent work [61] we reported a C/O ratio around 1.97 for aGO, close to the value 2 reported in [62,63]. The C/O ratio of 1.97 is the current value used in this paper. However, ODs compounds, characterized by high presence of oxygen moieties, have a lower C/O ratio with respect to aGO and bwGO. In particular, ODs are rich of carboxylated residues (e.g. carbonyl, carboxylic acids, and keto groups) as reported in [17], suggesting a possible structure for Oxidative Debris where carboxylated residues are mainly localized on the edges of the structure. However, these kinds of structures are strongly dependent on the synthesis method of the GO and any possible proposal of structure for ODs, although commendable, is certainly influenced by its own method of synthesis, so far from being considered unique and universal. The effect of the modulation of the C/O ratio on the optical properties of the GO can be obtained by using different concentrations of potassium permanganate ($KMnO_4$) in order to change the number of oxygen functionalities in the graphitic structure, increasing the oxidation grade of the GO, topic of our recent paper [64]. Regarding photo-emission, three main excitations mechanisms featuring PL spectra are $\sigma \rightarrow \sigma^*$ for photons excited at 200–230 nm, $n \rightarrow \pi^*$ (excitation wavelength ranging from 320 to 330 nm) and $\pi \rightarrow \pi^*$ (excitation wavelength ranging from 260 to 270 nm). GO with low oxidation degree showed a quite broad PL signal centered at 412 nm for λ_{exc}= 273 nm and very weak PL signal associated with the mechanism $n \rightarrow \pi^*$, meaning that few n-levels are available for recombination. By increasing oxidation degree much more n-levels appears due to the insert of oxygen groups (epoxy, hydroxyl, carbonyl and carboxyl groups) on the carbon basal plane, hence promoting a well-defined $n \rightarrow \pi^*$ transition which correspond to a red-shift in PL spectra. The effect of the base-washing on PL spectra of the GO with different oxidation grade was further studied. Starting from GO with low oxidation grade, the base-washing promotes the insert of -OH groups generating small sp^2 domains and trap-levels; for stronger oxidation grade, the removal of the oxygenated parts (most likely the ODs) takes place, restoring sp^2 coherent domains on the GO plane, in line with current literature. In this last case the availability of n-levels decreases for GO, but on the contrary, it increases for the removed oxygenated parts; hence the enhancement of the PLE band related to mechanism $n \rightarrow \pi^*$ for supernatant was observed. For this reason, it is worth mentioning that the C/O ratio of the starting graphene oxide impacts also on the effect of the base-washing. Finally, the increase of oxygen functionalities is usually confirmed by a blue-shift of the absorption band relative to $\pi \rightarrow \pi^*$ transition from 260 nm to 230 nm [64-67]. The origin of ODs has been subject of interest for some years by several authors, who have advanced the proposal that these structures are already present in the grid of the GO due to the strong oxidation by means of H_2SO_4 and $KMnO_4$ (typical reagents for Hummers synthesis); the subsequent alkaline washing separates the ODs from GO structure bringing them in solution [17-19,68,69]. Currently, this kind of model (two-component model) is widely accepted by the scientific community. Being rich in oxygen groups, the ODs are also responsible for some properties of the aGO as UV–Vis and IR absorption, electrochemistry, and photoluminescence; they represent with good probability 30% of the total mass of the pristine GO [15,70,71]. According to some authors, ODs could be bonded with their oxygen functionalities on the basal plane of GO by means of covalent bonds prefiguring a model where there is not separation between GO and ODs. On the other side, other authors [15, 18,19,63,69,72] state that the ODs interact with basal plane of the GO by means of non-covalent bonds mainly identified as π-π interactions among the two sp^2 planes. By following these conclusions, after basic treatment of the GO (named aGO) two components are obtained, the bwGO and the ODs. Generally, ODs are isolated by means of low-concentration basic solutions (NaOH or NH_4OH) at reflux but also in these cases different treatments are found in literature such as ultrasonication method [73]. The basic treatment should favourite the deprotonation of the ODs oxygen functionalities by making sure that these structures detach from the GO plane and a subsequent acidification of the aqueous solution up to pH 2–3 produced a protonation of the oxygens localized on the ODs promoting the precipitations of the ODs, as

brownish solid. Hence, the isolated ODs are characterized through the standard measurements such as TEM, XPS, FTIR, PL and UV–Vis. In according to many authors these characterizations lead to the unequivocal conclusion that ODs are already present in the structure of the GO, reducing the alkaline treatment to a simple washing or purification of the structure.

In opposite of these conclusions some authors [74] reported different results about the treatment of the GO in alkaline environment. In this last case, the authors argued that GO structure suffers a reduction process; disproportionation of the alcohol groups occurs in according with the scheme reported in [75], followed by a disintegration of the GO flakes. In this framework, the two-phases model becomes meaningless as well as the origin of the ODs which take on a meaning of simple fragments of graphene oxide derived from the grinding of its structure; the strong oxidized regions are those that, most likely, suffer a detachment from the sp^2 structure. These hypotheses could be rather real by considering that in GO the oxidized region which decorate the basal plane with oxygen moieties are characterized by the presence of sp^3 hybridized carbons and connected with sp^2 domains by means of covalent bond. In these frontier regions between sp^2 and sp^3 domains, it is most likely that the covalent bonds suffer a tensile stress due to the different hybridization of carbon atoms bonded together. Hence, also a mild alkaline hydrolysis could be sufficient to break the chemical bonds in these regions of borders. Moreover, as reported in [74], during the base-treatment, GO flakes cleave along the pathways specified by location of oxidized domains; most likely the pathways are localized where oxygen domains are bonded with sp^2 carbon. The C–C bonds can only be cleaved along the borders of the oxidized areas and the oxidized domains are distributed randomly. Finally, we would point out as the authors in [74] argued an interesting hypothesis in according to which during the basic treatment small point-like fragments of carbon are removed leaving holes on the GO plane. These fragments are not recognizable by TEM and SEM and are therefore not related to the ODs type structures because they are most likely too small. These ones cannot be isolated even after acidification, and they remain in the supernatant. In addition, their size become pronounced during a prolonged base treatment, leading to disintegration of the flakes into smaller pieces.

1.1. Overview on novelty of the paper

In this work we did not consider deeply the topic regarding the origin of these structures named ODs, since our work is limited to an observational approach of the photochemical behaviour of the GO when it is treated in an alkaline environment. Regardless of their origin, the nature of the ODs can be also related to that of the carbon quantum dots (CQDs) [17]. By considering the strict correlation among ODs and CQDs, it is natural to take account the exploiting of the light-emitting properties of these fragments for sustainable and low-cost application, for example, such as active material for luminescent devices. By the way, their optical properties were partially investigated in the past, in particular regarding absorption in UV–VIS region [19,62,71,72,76-79], although the conclusions and interpretations of the spectra are not always in agreement with each other. What is missing it is a clearer description of the emission properties. However, a possible reason of this misunderstanding of the results is an unclear nature of the ODs sample under analyse that we believe to be composed of two main components, one of these lighter and the other heavier. By considering the main three papers reporting fluorescent properties [19,71,79] of the GO and the role played by ODs, Hu reported a broad peak centered at 436 nm (blue emission) for N-doped GQDs (derived from ODs through hydrothermal process) together to other peaks with minor intensity which reveal a strong excitation dependent PL behaviour. In [71] two large peaks localized around 530 nm and 540 nm are recorded for excitation wavelength at 350 and 450 nm respectively which demonstrate, although for only two wavelengths, the excitation-dependent photoemission. In this last case the blue intensity is related to GO (unpurified and purified). However large peaks are a sign of the presence of many defects diffuse on the ODs surface. On the contrary, in [19] for ODs a strong emission was detected from blue emission (450 nm) to 530 nm, by using a 350 nm and 450 nm excitation wavelength respectively, and it is well visible in the PL-map. In [80] PL of the ODs was monitored as a function of pH. The ODs were stripped at different pH solution (after filtration with PTFE membrane) without further separation from the solution which leads different emission according with pH. For pH $>$ 10 a blue emission was recorded which corresponds to the typical emission of fulvic and humic acid-like components.

From our point of view the application and engineering of these nanostructured semiconductor for luminescent devices for example such as LEDs is hampered by a not yet very clear interpretation of spectroscopic data, since the alkaline treatment produces structures with different photoemitted behaviours. In function also of the previous cited papers, it is reasonable to define two main products from the base-washing of the GO, one of these are the ODs reported in literature. This fraction brown-coloured was obtained for precipitation after adding of acid up to reach pH 2–3. The other fraction is lighter, and it is not easily separable from native solution and reported in some references such as fulvic acid -like component. The latest has emissive component centred in the blue region much stronger than ODs fraction. Moreover, this lighter fraction continues to be produced in alkaline condition. That is, any further treatment of ODs under alkaline conditions (for example to study their photoluminescence at pH greater than 7) generates additional smaller and lighter fractions with strong blue-emission that interferes and sometimes overhangs the one that should be measured. Hence, we are interested to study what remains in the alkaline washing solutions after acidification, once it is gently separated from the brownish precipitate, which should be rich of the ODs. Surprisingly, we find a solution still strongly luminescent, also for mild alkaline treatment at room temperature, apparently free of material residues coming from GO structure and probably rich in specific molecular structures which could give support to a mechanism of disintegration of the pristine GO in opposite to the simple washing, or however to move in the direction towards a more likely combined mechanism. Specifically, we conducted several treatments of the GO prepared in the laboratory by using KOH, monitoring the alkaline processing with time for 15 min, 2 h, 4 h, 6 h, 8 h, 24 h, 30 h, 48 h, 72 h, 96 h. Generally, the time has never been taken in account as parameter in order to study the base-washing of the GO. Moreover, we showed that the base washing, in addition to the producing of ODs-related structures, could generate further lighter nanostructures with dual photoemission mechanism which suggests the presence of organic nanocluster chromophores as reported [81] or of large amount of fluorophores which play a role of building blocks of the carbogenic domains [82], in opposite to the generic fulvic acid -like components.

2. Experimental setup

The whole samples treated in this work were prepared by means of alkaline treatments of the graphene oxide. Alkaline agent is KOH (Carlo Erba Cas.No. 1310–58–3) and graphene oxide is prepared through modified Hummers method reported in [61]. Alkaline treatments were performed for different times reported in table 1. In particular, about 100 mg of GO were placed in 5 ml of KOH 0.1 M solution and subsequently 10 ml of H_2O distilled were added so that the final concentration of KOH is around 0.04 M. After a gently dissolution, the reaction followed under stirring at room temperature for the time reported in table 1. Subsequently, to separate the solid phase (named R1) from the liquid phase which should contain small GO fragments (named S1), the solutions were centrifugated at 4000 rpm for 15 min. By following the nomenclature in [15] R1 is named bw-GO and S1 contains the ODs dispersed in the aqueous solvent. The R1 residue (bw-GO) can be used for different applications; as example we used this powder in flexible sensors for humidity [83]. An amount of the native supernatants (named

Table 1
Experimental parameters time (in minute and hours), concentration (%) and volume (L) used for acidification the base washing solution rich of GO fragments (b). In Table 1a nomenclature of the products are reported.

a)

Native Supernatant	Base-washed GO	Acidified Supernatant	Second Residue (ODs)
Supernatant 1 S1	Sediment 1 R1	Supernatant 2 S2	Sediment 2 R2

b)

Samples	Times	H_2SO_4 (20%)	HCl (10%)
15min	15 min	500 μL	200 μL
2h	2 h	500 μL	
4h	4 h	500 μL	
6h	6 h	500 μL	
8h	8 h	500 μL	
24h	24 h	500 μL	
30h	30 h	500 μL	
48h	48 h	500 μL	
72h	72 h	500 μL	
96h	96 h	2000 μL	200 μL

S1), 3 mL, were acidified both with H_2SO_4 and HCl at room temperature (table 1) and left to sediment for 24–48 h at room temperature. After acidification, all the samples were further centrifuged at 4000 rpm for 15 min to recover the second residues (R2) which consist of heavy part of the ODs while the lighter component remain in the second acid supernatant (S2). In this work the residue R1 recovered after centrifugation was not taken into account.

Photoluminescence and optical absorption spectra of GO solutions were recorded by a FluoroMax 4 spectrofluorometer (Horiba Jobin Yvon, Edison, NJ, USA) and Cary 5000 UV–Vis-NIR (Agilent) Spectrophotometer using quartz cuvettes. Photoluminescence signals were reported as ratio S/R between the signal from sample S and the reference signal R with a bandpass of 3 nm. All the maps are recorded with step of 10 nm for excitations and 1 nm for emission unless it is otherwise indicated.

Vibrational Analysis was performed through a FTIR Nicolet™ iS™ 50 by Thermo Fisher Scientific, employing the ATR accessory equipped with a diamond crystal as internal reflection element (IRE). Spectra were recorded in absorbance ranging from 4000 to 400 cm^{-1} with 4 cm^{-1} in resolution.

3. Result and discussion

In Fig. 1a, we report two solutions after washing in KOH to stress the different colouring they have after different treatment times, in particular at 15 min (right) and 96 h (left) both at room temperature. In case of extended time the solution gets a colour even more brownish which could mean that the solution becomes more and more rich of GO fragments. The scheme of the process performed in this work is reported in Fig. 2.

The UV–Vis spectra (Fig. 3a) for S1_15min and S1_96h show a strong absorption around 240 nm together with the ones at 270, 310 nm and a shoulder around 210 and 350 nm, calculated from first derivative (at 240 and 270 nm the strength of the absorption is similar for both samples). It is worth noting that both signals rise very quickly for wavelengths decreasing towards 200 nm. These spectra are recorded by using diluted solutions (200 μl of solution in 2 ml of distilled water)like PL maps reported in Fig. 3b and c. Hence, by monitoring treatment times for short time (15 min) and longer time (96 h) there seems to be no relevant variation regarding the absorption wavelengths meanwhile the intensity feels a quite variability. Absorption bands calculated on the UV–Vis spectra are found at 240, 270 and 310 nm, corresponding to the absorption π→π* (240, 270 nm) and n→π* (310 nm).

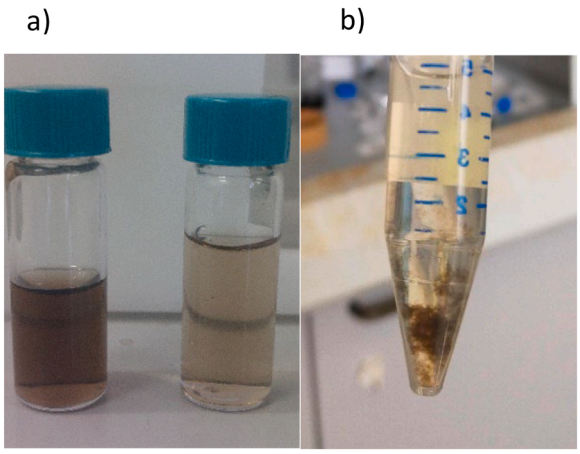

Fig. 1. Supernatant obtained after KOH treatment (1a) at 15 min (cuvette on the right) and 96 h (cuvette on the left), in order to show the effects of the extended treatment times on the GO fragmentation. After acidification a brownish coalescence appears at the bottom of the conical falcon (1b).

Figs.3b and 3c report PL maps for samples S1_15min and S1_96h and are recorded under the same dilution conditions. Starting from the UV region with λ_{ex} ranging for 240–250 nm, where the intensity of the excitation reaches the maximum (and where also the absorption is maximum), both samples have a maximum of emission at 450 nm and a tail, with similar intensity comparing the two samples, in the green up to red region. It is worth mentioning the good agreement among the absorption band in UV–Vis (in particular 270 and 310 nm) with the y-position of the two maximum contour levels in the PL maps (b,c). Both the two excitation wavelengths 270 nm and 310 nm induce blue emission approximately around 450 nm.

For native supernatant the emission excited by wavelengths λ_{ex} under 300 nm is inhibited by quenching effect (a strong absorption in that region is noticeable in Fig. 3a) and it emerges only for diluted samples (Fig. 3b and 3c), while for the more concentrated sample (Fig. 3d) only the emissions excited at λ_{ex} ~310–320 nm (λ_{em} ~450 nm) and λ_{ex} ~400 nm (λ_{em} ~505 nm) are evident. Table 2 shows λ_{em} as a function of the λ_{ex} for native and diluted supernatants, for the three transitions excited respectively at wavelengths around λ_{ex}=270 nm, 310–320 nm and 400 nm and giving emissions in the blue and green range.

For all the excitation wavelengths in the UV range the emission is generally detected at wavelengths around 450 nm and the position of the maximum slightly depends on the treatment time, as reported in Table 2; as the treatment time increases going from 15 to 96 min, λ_{ex} and the corresponding λ_{em} undergo a redshift.

Fig. 1SI in Supporting Information shows the effect of the dilution on S1_15min. The peak centered at λ_{ex} = 310 nm for no-diluted sample (1SIb) approximately corresponds to that of the diluted sample in Fig. 1SIa. Dilution makes less evident the weaker emission stimulated by excitation wavelengths around 400 nm. On the contrary, as it has to be expected from UV–Vis absorption spectrum, dilution allows to make evident the emission stimulated by λ_{ex} around 270 nm, clearly visible on the map for diluted S1_15min (Fig. 1SIa). In fact, optical absorption occurs especially in the deep UV region, so the system acts as a trap and prevents radiation from exiting and reaching the detector due to quenching effect. When the solution is diluted, the absorption effect is reduced, and photoluminescence excited in the UV region becomes detectable. On the other hand, the dilution effect makes disappearing some components, most likely those weaker. Therefore, considering the results of the two different maps reported in Fig. 1SI, we can argue that three different mechanisms accounts for the three emissions detected at λ_{ex}=270 nm, 310–320 nm and 400 nm, corresponding to the absorption band reported in Fig. 3a.

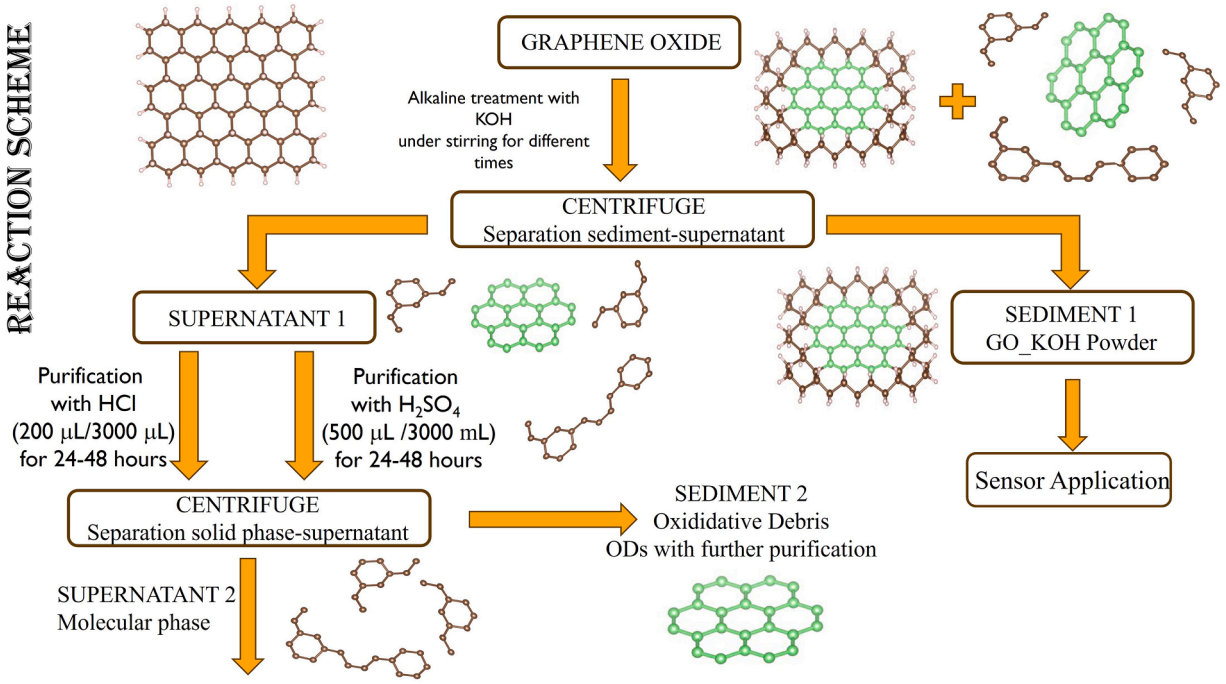

Fig. 2. Scheme of the alkaline treatment to obtain a lighter molecular phase which remain in the supernatant 2.

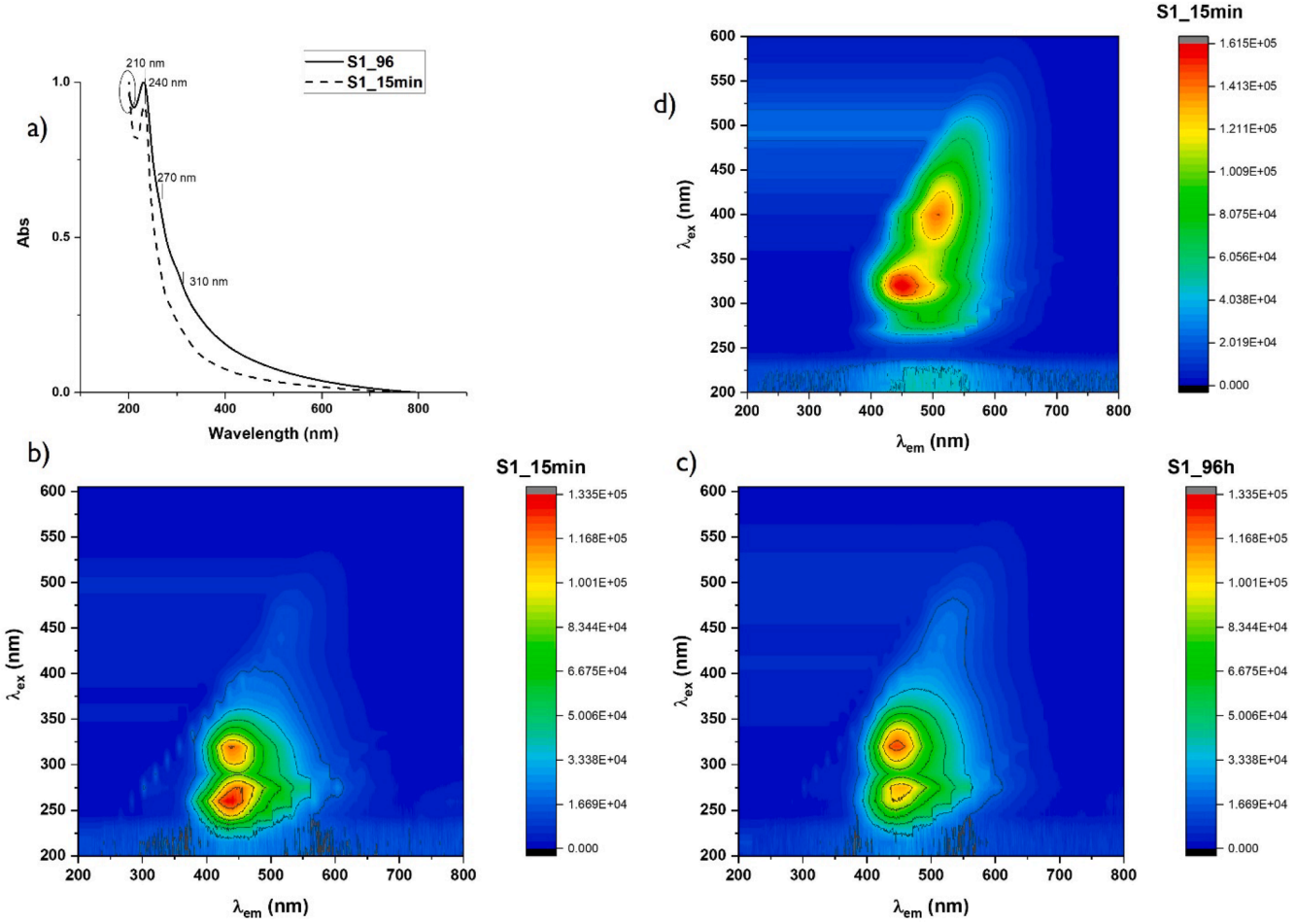

Fig. 3. UV–Vis spectra (a) and PL map (b-c) for sample S1_15min and S1_96h. The signal in b-c, are recorded with the same dilution factor used for UV–Vis absorption spectra and are reported with the same intensity scale; d) the map for sample S1_15min without dilution with its own scale different from that used for frames b) and c).

Table 2
λ_{em} in function of the λ_{ex} for native supernatant and diluted subsequently. In this case the emission under $\lambda_{ex} < 300$ nm emerges from quenching effect. All the values were correctly measured within ±1 nm. λ_{max} was reported in bold.

Sample S1	λ_{em} (λ_{ex} nm) Blue	λ_{em} (λ_{ex} nm) Blue	λ_{em} (λ_{ex} nm) Green
S1_15min	–	**450 (320)**	505 (400)
S1_96h	–	480 (370)	**530 (470)**
S1_15min (dil.)	**456(270)**	446 (310)	505 (410)
S1_96h (dil.)	454 (275)	**446 (320)**	505 (410)

Now, if we consider the effect of the treatment time on the mechanisms of photoluminescence in the visible range ($\lambda_{ex} > 400$ nm) (Fig. 4), photoluminescence (PL) maps of the supernatants without dilution show that excitation wavelengths, and consequently the corresponding emission, drift towards greater wavelengths with the treatment time. By comparing, for example, the S1_15min map with the analogous one recorded for longer exposure time to the alkaline treatment, we can see that the excitation wavelength giving the most intense emission signal shifts towards the visible range on the vertical axis and the corresponding maximum emission undergoes a red-shift. For prolonged time, the maximum of the intensity drifts at λ_{ex}~ 440–510 nm with emission from green to red (96 h). This trend of the PL signal could also be affected by a shielding effect (due to the increase of GO fragmentation) of the solution that becomes darker with increasing time (as seen in Fig. 1), reducing the number of emitted photons recorded by the detector.

By considering the profiles of the excitation spectrum reported in Fig. 5a for S1_15min, giving emission at 470 nm, they show signals with different excitation centres, at 280, 320, 375 and 400 nm (the maximum of PLE is centred at 320 nm). As the treatment time increases (S1_96h), the curve of excitation increases in the visible range. At the same time, if we consider the emission at 530 nm the effect of the prolonged treatment time clearly promotes the excitation in the range between 400 and 500 nm. This behaviour is explained by considering an increase in the carbonous fragments which detach from the GO in the alkalization phase and that abound in the liquid phase. Hence, taking in account two emitting components, one of this lighter, reasonably similar to the organic compound or polymer which has main excitation centres in the UV region, and one purely inorganic (with excitation centres mainly in the visible), we can assume that the prolonged time increases the presence of the inorganic fragments; these structures absorb in the blue region and emit in the green region with photoluminescent properties very similar to that found for Oxidative Debris or Carbon Quantum Dots. For the sample obtained after 96 h of treatment the maximum excitation is got in the blue region where PLE curve has the features of a continuous band, that in our opinion, can be due to the presence of a huge number of carbonous pieces. The lighter phase having maximum excitation in the blue range remains constant with the treatment time as it has formed in the first moments of the treatment.

In Fig. 5b the emission bands are measured for λ_{ex}=320 nm (solid lines) and λ_{ex}=470 nm (dashed lines) for both samples but, as it can be noted, λ_{ex}=320 nm gives the maximum emission for sample S1_15 min in the blue range, while λ_{ex}=470 nm gives the maximum emission for S1_96h in the green range (see table 2). Moreover, if we consider the empirical ratio of the maximum PL emission excited at 320 nm and 470 nm I_{320}/I_{470} for both sample S1_15min and S1_96h, it can be seen that for 15 min we obtain a ratio of 2.3 which becomes 0.4 for the sample 96h.

Fig. 2SI clearly shows the dependence of the emission in function of the excitation wavelengths for S1_15min sample.

For diluted supernatants S1, the PL signals excited in the UV are

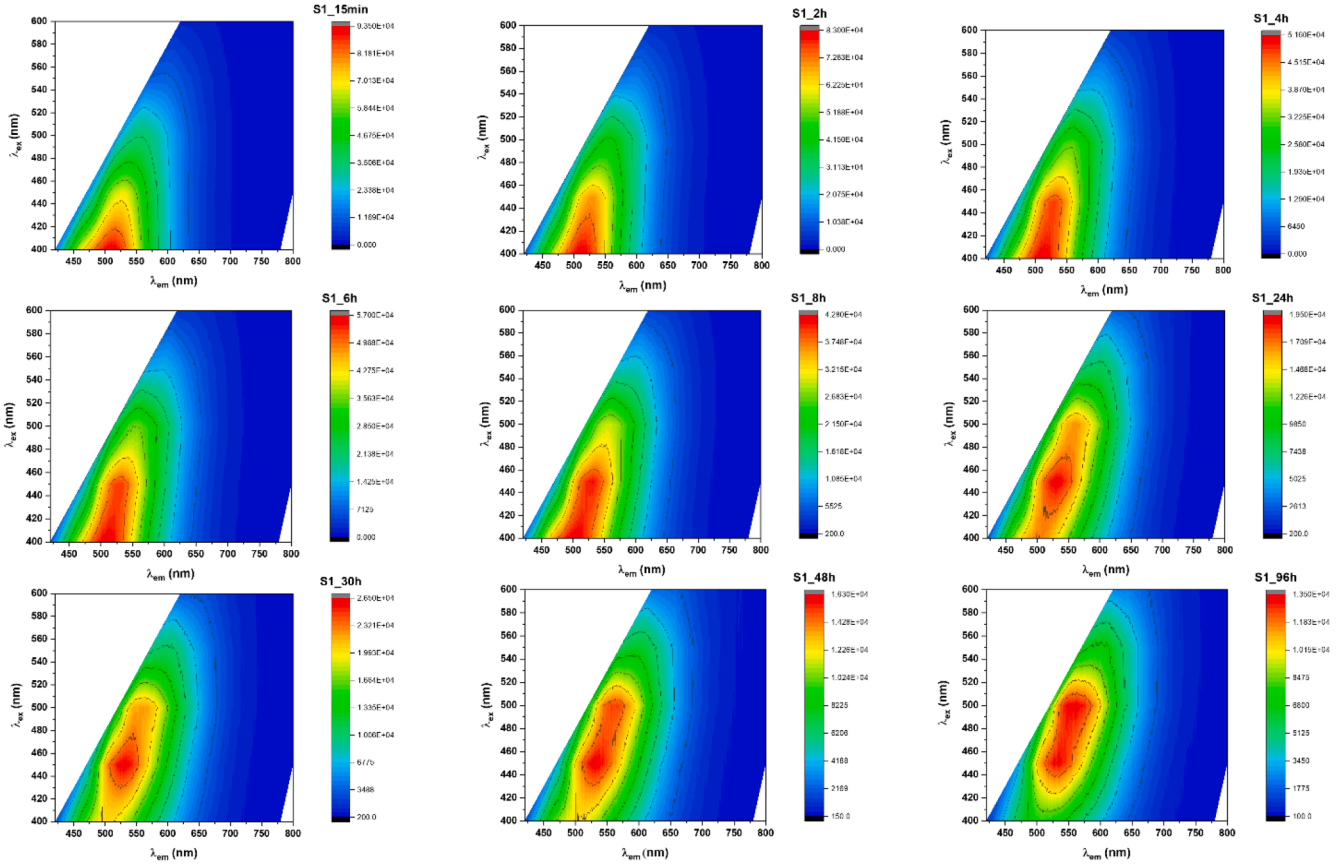

Fig. 4. PL maps for all the samples of supernatants recovered from GO treatments in alkaline solution recorded for emission and excitation wavelengths ranging for 400–800 nm and 400–600 nm respectively with step of λ_{ex}=50 nm. Each figure is reported on own scale.

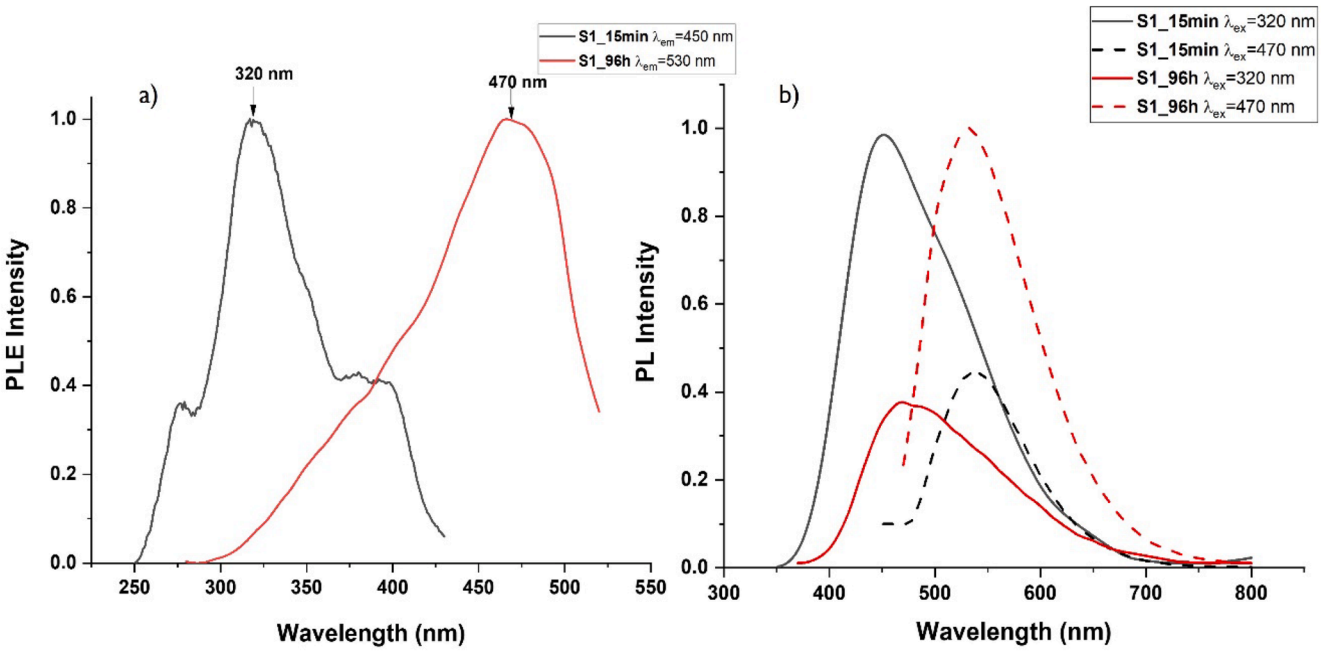

Fig. 5. Excitation spectra (a and b) for samples 15 min and 96 h normalized. In this context, the ratio I_{320}/I_{470} for sample 15 min is 2.3 while for 96 h is 0.4. All the spectra reported here belong to the native samples without dilution.

centered around the values which do not suffer significative shifts with respect the treatment time. Its maximum depends on excitation wavelength, and it is found for $\lambda_{max} < 300$ nm. In this case, the emission peaks at higher wavelengths (green-luminescence) are very weak as we can see in Fig. 3(b and c).

After additional acidification by adding of H_2SO_4 and centrifugation, we obtained second supernatants (named S2) whose characteristic PL maps (Fig. 3SI) show contours with highest intensity approximately in the same wavelength range for all the samples, around 450 nm in emission and 320 nm in excitation. With respect to the native supernatant before acidification, we did not record any drift toward higher wavelengths with increasing treatment time. No strong emission in the green region (for λ_{ex} in the blue range) was detected in S2 as if the removal of the heavier GO fragments from S1(the ODs) is responsible for the elimination of that emission in the green, leaving just a little tail. Hence, if we proceed to the dilution (200 μL for 2000 μL) also for the second supernatants (even though they already undergo a dilution effect due to the acidification), once again, the highest PL emission intensity is induced by two excitation wavelengths centered around 320 nm and 270 nm, which appears only after dilution in water (Fig. 4SI). The maps reported in Fig. 4SI for diluted S2_15min and S2_96h are substantially similar to the maps in Fig. 3b and c for S1. However, while the weak photoluminescence excited by blue stimulation appears for the concentrated sample S1, for S2 it does not appear neither concentrating the solution. We therefore faced to the elimination of components which give emission at higher wavelength for effect of the dilution in the case of S1 and a removal effect of heavy fragments in the case of S2. In both cases, therefore, for S1 and S2 to see the blue-luminescence with excitation in the far UV (260–270 nm) a strong dilution in water is necessary. These considerations conduct to think that in S1 and again in S2 after acidification there is a lighter phase with a strong absorption in the far UV and strong blue-emission, most likely remaining unchanged in the two supernatants which is not removed during treatment from S1 to S2.

Moreover, after acidification, we see that the maximum emission occurs at about λ_{max}~450 nm wavelength, similarly to that obtained for native supernatants. In addition, although there is a not negligible contribution of emission in the green region, this contribution remains constant with respect to the treatment time (see data in Table 3) and

Table 3
λ_{em} in function of the λ_{ex} for supernatant S2 after acidification and dilution. We report λ_{em} relatively to three emission regions (λ_{max} in bold), with an error within ± 1 nm.

Sample S2	λ_{em} (λ_{ex} nm) Blue	λ_{em} (λ_{ex} nm) Blue	λ_{em} (λ_{ex} nm) Green
S2_15min	–	**450 (330)**	500 (410)
S2_96h	–	**450 (320)**	500 (410)
S2_15min (dil.)	**454(270)**	445(320–330)	505(410)
S2_96h (dil.)	**452 (275)**	445(320)	505(410)

there is no significant variation in intensity. In addition, Fig. 5SI(a) shows a dual photoemission mechanism for the supernatants S2, in this case S2_96h sample. Specifically, an independent-excitation wavelength component is observed for λ_{ex} ranging from 275 nm to 335 nm (far UV) while a dependence of emission wavelength has been identified for λ_{ex} closer to visible range, in particular from 350 nm to 500 nm. This photoemission behaviour suggests the presence of more complicated nature of S2: reference [82] showed that carbogenic nanostructures arising from thermal decomposition of citric acid have this emission behaviour, in function of temperature. In particular, at low decomposition temperature the independent-excitation component prevails, most likely due to the large number of fluorophores moieties building the nanoparticles. On the contrary, at higher temperature carbon nanoparticles are formed with carbogenic cores which are the main source of their PL, inducing an excitation-dependent emission, typical of CQDs, toward longer wavelength and with systematic decrease of the intensity. Fig. 5SI(b) showed yellow fluorescence excited with 532 nm laser diode emitted by S1_96h(left and centre figure) and S2_96h(right) samples. S1_96h is the native supernatant before purification and a large amount of oxidative fragments with emission of green light characterizes this sample fraction. In fact, the 532 nm laser diodes passes through quartz cuvette and a white light is produced inside the cuvette, most likely due to scattering of photons derived from the source plus additional components (yellow and probably red). The same experiment was carried out (figure b in the centre) by placing a filter for green light at (570 nm) between cuvette and observer. In this case, a fluorescent yellow light is clearly visible, eliminating the contribution of the laser source. Then, the

same yellow fluorescence is detectable in the sample S2_96h (right) without placing any filter. Hence, it is most likely that the purification with acid removes most of the heavier fragments (ODs) which played the role of scattering centres for green light, leaving only the lighter fraction which absorbs and converts most of the green photons in yellow fluorescence. Figure c showed PL emission (by using spectrofluorometer) of S2_96 h for λ_{ex} =530 nm. A similar behaviour was found in [81] for complex organic nanoparticles whose photoluminescence was due to the self-assembly chromophore molecules rich of alcohol and ester carbonyl groups.

Fig. 6SI shows the behaviour of the PL in function of λ_{ex} for diluted S1_15min and S2_15min samples. For wavelength greater than 300 nm (b,c,e,f) we found a behaviour similar to carbon quantum dots where PL is dependent on λ_{ex} and a red-shift of the λ_{max} is clearly shown due to the quantum confinement. This trend seems not to be confirmed for excitation lower than 300 nm (a,d).

In Fig. 6 we found similar behaviour for the sample treated for 96 h but we reported also PL of the sediment R2 which we have recovered in abundance after acidification as a residue powder. For R2 (g,h,i) the PL emission is peaked at λ_{max} greater than 500 nm (excited at λ_{ex} greater than 230 nm). This fact confirms that after protonation with acid many fragments coming from disintegration of GO and removed from supernatants are emitters with green-luminescence and most likely they were the source of the shift toward green emission with treatment time recorded in the maps of Fig. 4. These signals in the green range are visible in native supernatants but they are very weak after dilution. The tails of the green-emission which appear in the supernatants S2 after removal of the sediment R2 can be due to the fragments R2 residuals, or mechanisms of photoluminescence very weak present also in the lighter emitters. After all, the nature of R2 and S2 should be similar because both come from the same structure.

Finally, UV–Vis spectrum for 15 min reported in Fig. 7a, compare three signals, native supernatant (S1_15min), acidified supernatant (S2_15 min) and the solid residue after acidification (R2_15min). S1_15min and S2_15 min have almost the same absorption peaks at the same wavelength for $\lambda_{abs} < 300$ nm, in particular 240, 270 and 320 nm, including the shoulder at 210 nm. R2_15min is characterized by only one weak signal widespread around 270 nm, while the shoulder at 210 nm is absent. This last signal is important because it is the region of absorption by benzene rings associated to the presence of fulvic and humic acid, as reported in [78,84], hence of structures lighter than ODs. Although there is not much information about UV–Vis of ODs, by following De Lima but also our recent work [64] the absorption at 270 nm is typical for π-π* absorption band, as example for bw-GO, and it can be common for S1, S2 and R2 being all structures characterized by aromatic planes. The strong absorption at 240 nm can be attributed to electronic transition involving oxygen groups different with respect to those bonded in the R2 residue which has not absorption in that region of the spectrum. The UV–Vis spectra of the ODs reported for example in [15,78,85] show the strong absorption at 210 nm but in our opinion this signal belongs to lighter phase which has blue-photoluminescence meanwhile the heavier component which has green-luminescence (R2) does not show this signal and shows a single absorption around 270 nm. The spectrum reported in [85] seems to be similar to our S2.

Furthermore, in order to check the effect of the sulphate ions we performed purification of the supernatants S1 by using HCl instead H_2SO_4 without finding significant differences. A HCl 10% solution reduces the pH of the supernatants approximately to the same values of the H_2SO_4 acidification. For sake of completeness, some results about PL and UV–Vis spectra are reported in Fig. 7SI. Regarding these differences, it is worth mentioning the absorption at 210 nm in UV–Vis spectra, much more pronounced with respect the signal of the H_2SO_4 acidified

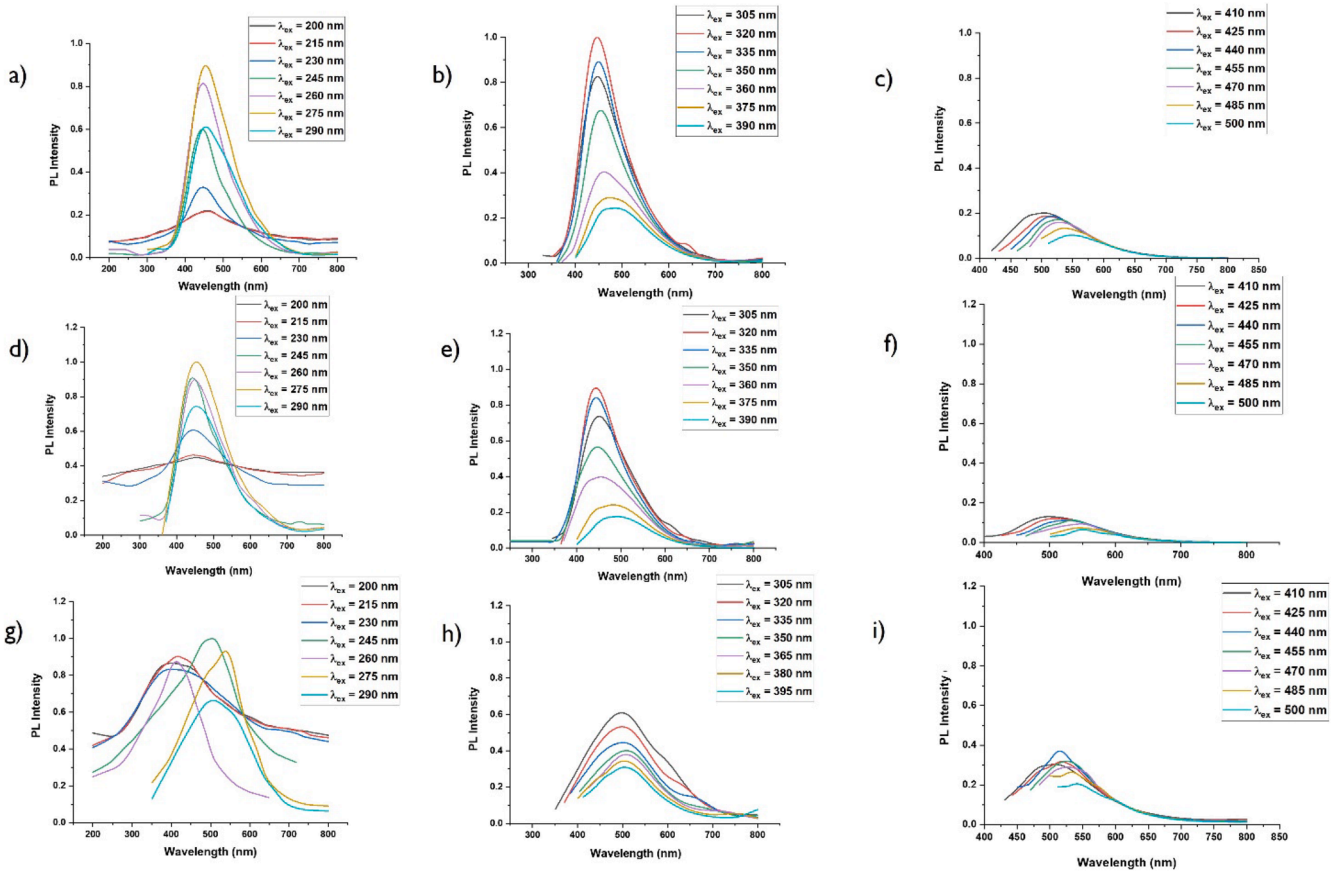

Fig. 6. PL in function of excitation for diluted S1_96h (a,b,c) and S2_96h (d,e,f) together with R2_96h (g,h,i).

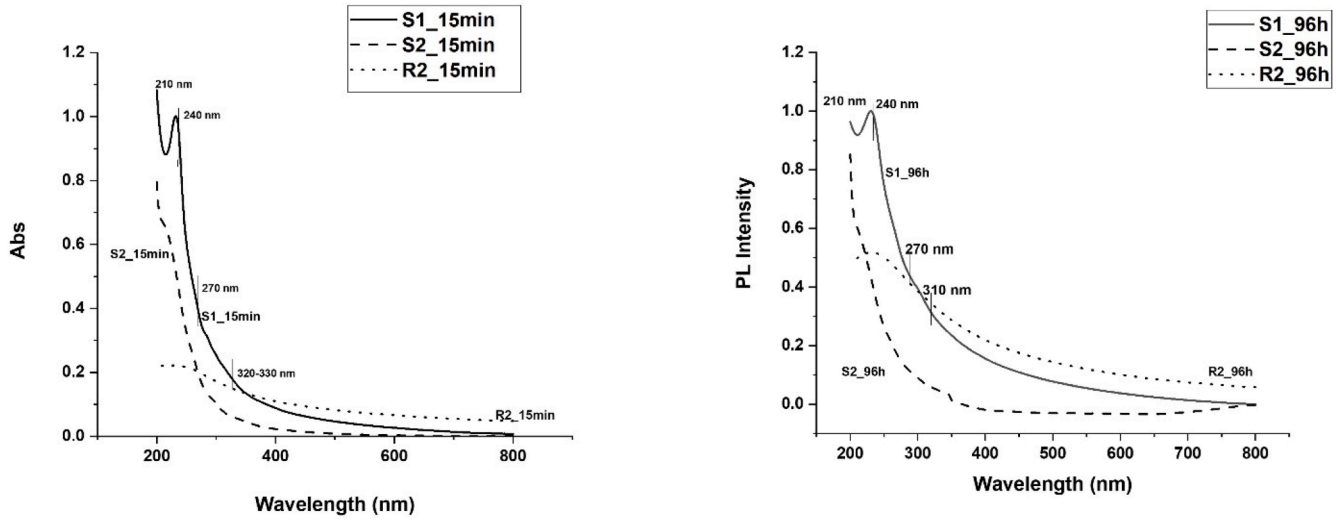

Fig. 7. UV–Vis spectra for samples 15 min and 96 h.

supernatants, as if chloride ions interfere with the absorption signal at those wavelengths.

Finally, we report vibrational analysis performed for S1, R1, S2 and R2. As you can see in Fig. 8SI, the residues R1 (which are GO powder after alkaline treatment) have the same absorptions without showing any particular differences with respect native GO. The absorption bands are those traditional ones reported in literature. Although FTIR is not a quantitative analysis, it is worth noting as the intensity ratio between C=C and C=O bands is shifted towards an increase in absorption C=C compared to C=O for samples after treatment in KOH. This could mean that part of the C=O ends up in the supernatants. Fig. 8SI shows that at first approximation, as for R1, the effect of prolonged time on the alkaline treatment of GO does not produce significant differences regarding functional groups; hence, the only thing it produces is the increase in solution of the fragments of GO with green-emission. Since FTIR signals do not change with exposure time, in Fig. 8 main absorption band were reported for S1, S2 and R2 samples treated for 15min.

Frequencies are reported in Fig. 8a and b and with corresponding absorption specie in Table 4.

We found stretching modes of the methyl and methylene groups (4a) which are not reported generally in the literature but that could have a more relevant role for understanding these structures. Furthermore, the absorption at 1730 cm^{-1}, corresponding to the carbonyl group of esters, lactones, carboxylic acids, aldehyde and ketones, has a strong intensity particularly for R2 hence for those inorganic fragments which we believe to be similar to the ODs. This peak is rather large hence it can contain more than one of the carbonyl structures. As reported in [15,17] ODs are rich structures of oxygen moieties such as carbonyl and carboxyl groups. Moreover, the band at 1394 cm^{-1} can be associated to the O—H bending of the carboxyl group, which is detected for S1, the native supernatant; the supernatant S2 which contains the lighter phase of the emitters seems do not have this absorption while for R2 it is slightly shifted at 1380 cm^{-1}. The same band can be associated to O—H bending of phenols hence S2 could be poor of aromatic groups as it can see also for the weaker absorption of C=C aromatic at 1594 cm^{-1} which is stronger for S1 and R2. All the other absorptions are those typical of these structures derived from GO, therefore ethers and primary alcohols which absorb at similar wavelength, hence secondary and tertiary alcohols. The latest, which we found in S1, belong mainly to the ODs while ethers, secondary and primary alcohols were found for all the structures.

Finally, for absorptions under 1000 cm^{-1} the bands around 958 cm^{-1} and 616 cm^{-1} correspond to the bending out of plane and in plane of the

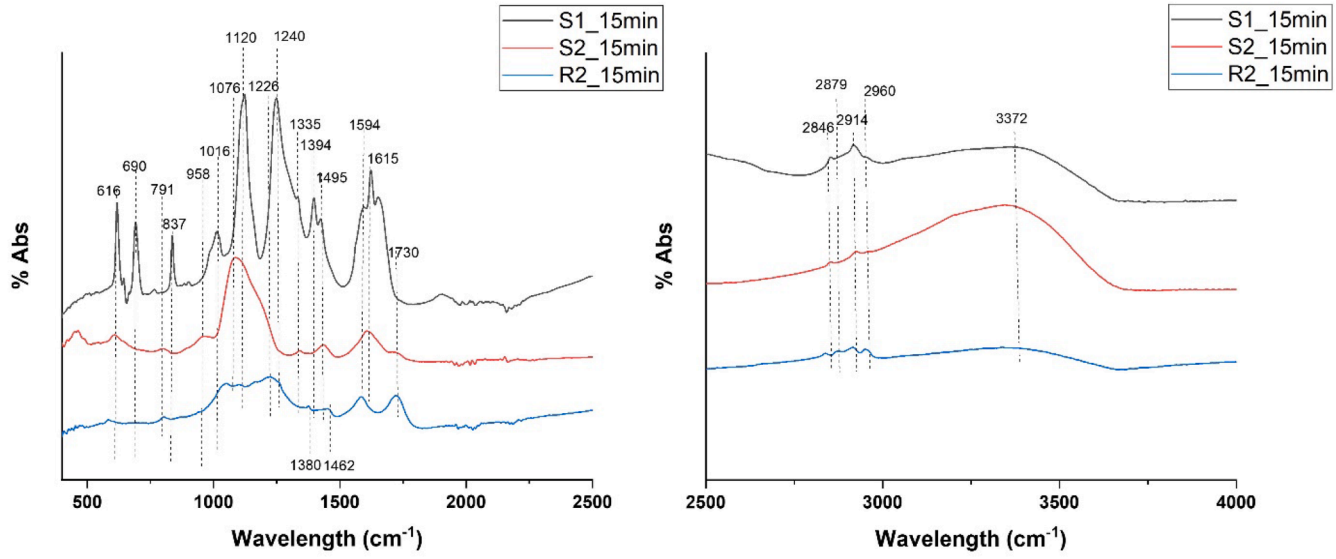

Fig. 8. FT-IR spectra for samples treated at 15 min and 96 h.

Table 4
FT-IR absorption band regarding S1, S2 and R2 treated at 15 min. In 4a υas and υ*sym* are symmetric and asymmetric stretching.

a)

cm^{-1}	3372	2960	2914	2879	2846
S1_15min	υ O−H	υas C-H_3	υas C-H_2	υsym C-H_3	υsym C-H_2
S2_15min	υ O−H	υas C-H_3	υas C-H_2	υsym C-H_3	υsym C-H_2
R2_15min	υ O−H	υas C-H_3	υas C-H_2	υsym C-H_3	υsym C-H_2

b)

cm^{-1}	1730	1615	1594	1394	1335	1240	1226	1120	1076	1016	958	616
S1_15min	υC=O	υC=C	υC=C Ar	υCOOH	υS=O	υC−OH t.	–	υC-OH s.	–	υC-O-C	–	δC-C-C
S2_15min	υC=O	υC=C	–	–	υS=O	–	υC-O	υC-OH s.	υC-O-C	–	δC-C-C	δC-C-C
R2_15min	υC=O	–	υC=C Ar	υCOOH	–-	υC−OH t.	υC-O	υC-OH s.	υC-O-C	–	–	δC-C-C

aromatic ring respectively. At 690, 791 and 837 cm^{-1} are most likely the C—H strain out of the ring. In our opinion FTIR analysis performed on these kinds of samples must be considered as average measures, that is, a band absorption is such only as an average of absorptions on every single structure present in the sample, but it is not really true that every single structure in the sample has that specific absorption and therefore possesses that specific functional group.

4. Conclusion

We have shown a gently alkaline treatment (0.04 M, Room Temperature) of the GO which produces, two emitting components in the visible spectrum; one lighter (S2) and another heavier (inorganic) (R2) having blue and green emission respectively, verified by measuring their PL and PLE. The lighter component is always present both in S1 and S2 supernatants independently on the time of reaction. On the contrary the heavier one is removed after acidification and precipitates in the residue R2; this observation is warranted by PL blue and green-emissions: while for S1_96h emission goes from 480 nm to 530 nm, for S2_96h, obtained as supernatant after acidification, it goes from 450 to 500 nm which are similar to the values obtained for the sample S1_15min where very few heavier residues have been produced. It is worth pointing out that 530 nm is the maximum PL emission for S1_96h which was lost both after acidification or alternatively, as discussed in the text, for dilution. In any case both component S2 and R2 have PL emission tails in green and blue respectively which make it difficult to discriminate sharply the heavier and lighter components in the two samples. Hence, our procedure, which uses a mild recover of R2 after acidification by gravity at room temperature without reflux, allows to separate these components even though the lighter one remains in solution and currently we are not able to separate it from aqueous solvent in order to more deeply analyse it. We showed that the base washing could generate further lighter nanostructures with dual photoemission mechanism which suggests the presence of organic nanocluster chromophores as reported [81] or of large amount of fluorophores which play a role of building blocks of the carbogenic domains [82]. The innovation and the research of novel materials with luminescent properties such as organic and polymeric fluorescent nanoparticles have received considerable attention because of their potential applications, including material sciences, biology, biomedicine, diagnostic and therapeutic treatment due to some of their advantages including a low biological toxicity and being environmentally friendly [86]. Moreover, novel luminescence mechanisms are being studied, such as aggregated induced emission (AIE) or clustering-trigged emission (CTE) in order to have molecules with better biocompatibility, lower cytotoxicity and mutagenicity compared to conjugated and aromatic counterparts [87-89]. For example, CTE mechanism is based on the aggregation of heteroatoms such as O, S and N bonded such as -C=O, -CN, -CONH- and -OH groups among others. The shorter distance enhances the spin-orbital coupling and the production of triplet states involved in photoemission mechanisms[87]. Unconventional emissive fluorophores can be biomaterials obtained from waste biomass, dendrimers, polyamides or amino acids and in general structures which do not necessarily have conjugated or aromatic nature [86,90], allowing to enlarge the range of structures photon emitters. Moreover, it is appropriate taking care also of the synthesis methods that must be increasingly sustainable, with low environmental impact and without the use of critical materials.

The specific causes of the PL emission in this type of materials are yet unclear and many efforts were done in order to understand better these novel features [91-93]. Given the clustering and the presence of many functional groups with heteroatoms (in particular O and N) linked to the oxidative debris, it is our opinion to address the studies about emissive properties of the ODs also in this direction.

Consent to publish

All authors have read and agreed to the published version of the manuscript.

CRediT authorship contribution statement

Emiliano Burresi: Writing – original draft, Validation, Methodology, Investigation, Formal analysis, Data curation, Conceptualization. **Maria Lucia Protopapa:** Writing – original draft, Validation, Supervision, Methodology, Formal analysis, Data curation.

Declaration of competing interest

The authors declare that they have no known competing financial interests or personal relationships that could have appeared to influence the work reported in this paper.

Supplementary materials

Supplementary material associated with this article can be found, in the online version, at doi:10.1016/j.cartre.2024.100412.

Data availability

No data was used for the research described in the article.

References

[1] M.A. Delucchi, C. Yang, A.F. Burke, J.M. Ogden, K. Kurani, J. Kessler, D. Sperling, Emissions, petroleum use, material use, lifetime infrastructure requirements, greenhouse-gas An assessment of electric vehicles: technology, cost, consumer acceptance and policy initiatives, Phil. Trans. R. Soc. A 372 (2014) 20120325, https://doi.org/10.1098/rsta.2012.0325.

[2] C. EL Latunussa, K. Georgitzikis, C. Torres de Matos, M. Grohol, U. Eynard, D. Wittmer, L. Mancini, M. Unguru, C. Pavel, S. Carrara, F. Mathieux, D. Pennington, G.A. Blengini, Study On the EU's List of Critical Raw Materials (2020), Publications Office of the European Union, Luxembourg, 2020, https://doi.org/10.2873/92480.

[3] A.D. Jara, A. Betemariam, G. Woldetinsae, J.Yong Kim, Purification, application and current market trend of natural graphite: a review, Int. J. Min. Sci. Technol. 29 (2019) 671–689, https://doi.org/10.1016/j.ijmst.2019.04.003.

[4] N. Deprez, D.S. McLachlan, The analysis of the electrical conductivity of graphite conductivity of graphite powders during compaction, J. Phys. D: Appl. Phys. 21 (1988) 101, https://doi.org/10.1088/0022-3727/21/1/015.

[5] A. Ambrosi, C.K. Chua, N.M. Latiff, A.H. Loo, C.H.A. Wong, A.Y.S. Eng, A. Bonanni, M. Pume, Graphene and its electrochemistry – an update, Chem. Soc. Rev. 45 (2016) 2458–2493, https://doi.org/10.1039/C6CS00136J.

[6] A. Ferrari et, Science and Technology roadmap for graphene, related two-dimensional crystals and hybrid systems, Nanoscale 7 (2015) 4587–5062, https://doi.org/10.1039/c4nr01600a.

[7] G. Eda, M. Chhowalla, Chemically derived graphene oxide: towards large-area thin-film electronics and optoelectronics, Adv. Mater. 22 (2010) 2392–2415, https://doi.org/10.1002/adma.200903689.

[8] R. Maheswaran, B.Prabu Shanmugavel, A critical review of the role of carbon nanotubes in the progress of next-generation electronic applications, J. Electron. Mater. 51 (2022) 2786–2800, https://doi.org/10.1007/s11664-022-09516-8.

[9] Z. Zhang, J. Zhang, N. Chen, L. Qu, Graphene quantum dots: an emerging material for energy-ralted applications and beyond, Energy Environ. Sci. 5 (2012) 8869, https://doi.org/10.1039/e2ee22982.

[10] L. Tang, R. Ji, X. Cao, J. Lin, H. Jiang, X. Li, K.S. Teng, C.M. Luk, S. Zeng, J. Hao, S. P. Lau, Deep ultraviolet photoluminescence of water-solube self- passivated graphene quantum dots, ACS. Nano 6 (2012) 5102–5110, https://doi.org/10.1021/nn300760g.

[11] M.S. Mehata, S. Biswas, Synthesis of fluorescent graphene quantum dots from graphene oxide and their application in fabrication of GQDs@AgNPs nanohybrids and sensing H_2O_2, Ceram. Int. 47 (2021) 19063–19072, https://doi.org/10.1016/j.ceramint.2021.03.252.

[12] M. Fu, F. Ehrat, Y. Wang, K.Z. Milowska, C. Reckmeier, A.L. Rogach, J. K. Stolarczyk, A.S. Urban, J. Feldmann, Carbon dots: a unique fluorescent cocktail of polycyclic aromatic hydrocarbons, Nano Lett. 15 (2015) 6030–6035, https://doi.org/10.1021/acs.nanolett.5b02215.

[13] L. Wang, S.-J. Zhu, H.-Y. Wang, S.-N. Qu, Y.-L. Zhang, J.-H. Zhang, Q.-D Chen, H.-L. Xu, W. Han, B. Yang, H.-B. Sun, Common origin of green luminescence carbon nanodots and graphene quantum dots, ACS. Nano 8 (2014) 2541–2542, https://doi.org/10.1021/nn500368m.

[14] P. Blyweert, V. Nicolas, V. Fierro, A. Celzard, 3D printing of carbon-based materials: a review, Carbon. N. Y. 183 (2021) 449–485, https://doi.org/10.1016/j.carbon.2021.07.036.

[15] A.H. de Lima, I. Scarpa, N.C. Lima Azevedo, G.C. Lelis, M. Strauss, D.S.T. Martinez, R.F. de Oliveira, Oxidative debris in graphene oxide: a decade of research, J. Mater. Chem. C 11 (2023) 12429–12452, https://doi.org/10.1039/D3TC02057F.

[16] J.P. Rourke, P.A. Pandey, J.J. Moore, M. Bates, I.A. Kinloch, R.J. Young, N. R. Wilson, The real graphene oxide revealed: stripping the oxidative debris from the graphene-like sheets, Angew. Chem. Int. Ed. 50 (2011) 3173–3177, https://doi.org/10.1002/anie.201007520.

[17] X. Chen, B. Chen, Direct observation, molecular structure, and location of oxidation debris on graphene oxide nanosheets, Environ. Sci. Technol. 50 (2016) 8568–8577, https://doi.org/10.1021/acs.est.6b01020.

[18] H.R. Thomas, S.P. Day, W.E. Woodruff, C. Valles, R.J. Young, I.A. Kinloch, G. W. Morley, J.V. Hanna, N.R. Wilson, J.P. Rourke, Deoxygenation of graphene oxide: reduction or cleaning? |Chem. Mater. 25 (2013) 3580–3588, https://doi.org/10.1021/cm401922e.

[19] H.R. Thomas, Cristina Valles, R.J. Young, I.A. Kinloch, N.R. Wilson, J.P. Rourke, J. Mater. Chem. C 1 (2013) 338, https://doi.org/10.1039/c2tc00234e.

[20] B. Brodie, On the atomic weight of graphite, Philos. Trans. R. Soc. London 149 (1859) 249–259.

[21] L. Staudenmaier, Berichte der Dtsch, Chem. Gesellschaft 31 (1898) 1481–1487.

[22] J. William, S. Hummers, R.E. Offeman, Preparation of graphite oxide, J. Am. Chem. Soc. 80 (1958) 1339, https://doi.org/10.1021/ja01539a017.

[23] R. Verdejo, S. Lamoniere, B. Cottam, A. Bismarck, M. Shaffer, Removal of oxidation debris from multi-walled carbon nanotubes, Chem. Commun. (2007) 513–515, https://doi.org/10.1039/b611930a.

[24] A.F. Faria, D. Stéfani T. Martinez, A.C.M. Moraes, M.E.H. Maia da Costa, E. B. Barros, A.G. Souza Filho, A.J. Paula, O.L. Alves, Unveiling the role of oxidation debris on the surface chemistry of graphene through the anchoring of Ag nanoparticles, Chem. Mater. 24 (2012) 4080–4087, https://doi.org/10.1021/cm301939s.

[25] X. Huang, Z.Y. Yin, S.X. Wu, X.Y. Qi, Q.Y. He, Q. Zhang, Q.Y. Yan, F. Boey, H. Zhang, Graphene-based materials: synthesis, characterization, properties, and applications small 7 (2011) 1876–1902. 10.1002/smll.201002009.

[26] V. Singh, D. Joung, L. Zhai, S. Das, S.I. Khondaker, S. Seal, Graphene based materials: past, present and future, Prog. Mater. Sci. 56 (2011) 1178–1271, https://doi.org/10.1016/j.pmatsci.2011.03.003.

[27] G. Eda, M. Chhowalla, Chemically derived graphene oxide: towards large-area thin-film electronics and optoelectronics, Adv. Mater. 22 (2010) 2392–2415, https://doi.org/10.1002/adma.200903689.

[28] X. Fan, W. Peng, Y. Li, X. Li, S. Wang, G. Zhang, F. Zhang, Deoxygenation of exfoliated graphite oxide under alkaline conditions: a green route to graphene, Preparation Adv. Mater. 20 (2008) 4490–4493, https://doi.org/10.1002/adma.200801306.

[29] P.P. Brisebois, M. Siaj, Harvesting graphene oxide – years 1859 to 2019:a review of its structure, synthesis, properties and exfoliation, J. Mater. Chem. C 8 (2020) 1517–1547, https://doi.org/10.1039/c9tc03251g.

[30] N. Bellier, P. Baipaywad, N. Ryu, J.Y. Lee, H. Park, Recent biomedical advancements in graphene oxide- and reduced graphene oxide-based nanocomposite nanocarriers, Biomater. Res. 26 (2022) 1–23, https://doi.org/10.1186/s40824-022-00313-2.

[31] D. Bose, G.A. Kaur, S. Balayan, S. Chatterjee, A. Tiwari, The logic devices for biomolecular computing: progress, strategies, and future directions, Nano Today 57 (2024) 102320, https://doi.org/10.1016/j.nantod.2024.102320.

[32] N. Sharma, D. Yadav, M.I. Hassan, C.M. Srivastava, S. Majumder, A review on exploring the impact of graphene oxide-based nanomaterials on structures and bioactivity of proteins, J. Mol. Liq. 404 (2024) 124980, https://doi.org/10.1016/j.nanoso.2024.101282.

[33] A.D. Sontakke, S. Tiwari, M.K. Purkait, A comprehensive review on graphene oxide-based nanocarriers: synthesis, functionalization and biomedical applications, FlatChem 38 (2023) 100484, https://doi.org/10.1016/j.flatc.2023.100484.

[34] M.Al Kausor, D. Chakrabortty, Graphene oxide based semiconductor photocatalysts for degradation of organic dye in waste water: a review on fabrication, performance enhancement and challenges, Inorg. Chem. Comm. 129 (2021) 108630, https://doi.org/10.1016/j.inoche.2021.108630.

[35] J. Campos-Delgado and M.E. Mendoza, Ternary graphene oxide and titania nanoparticles-based nanocomposites for dye photocatalytic degradation: a review materials 17 (2024) 135. https://doi.org/10.3390/ma17010135.

[36] S. He, Y. Ma, G. Maulik, M. Jellicoe, A. Nag, W. Powell, S. Deng, J. Fang, Y. Wu, A review on graphene-based sensors for tactile applications sensors & actuators: A, Physical 372 (2024) 115363, https://doi.org/10.1016/j.sna.2024.115363.

[37] S. Tang, Z. Liu, Xu Xiang, Graphene oxide composite hydrogels for wearable devices, Carbon Lett. 32 (2022) 1395–1410, https://doi.org/10.1007/s42823-022-00402-1.

[38] K. Nishshankage, A. Breverly Fernandez, S. Pallewatta1, P.K.C. Buddhinie, and M. Vithanage, Current trends in antimicrobial activities of carbon nanostructures: potentiality and status of nanobiochar in comparison to carbon dots Biochar 6 (2024) 2. https://doi.org/10.1007/s42773-023-00282-2.

[39] Rashi, Exploring the methods of synthesis, functionalization, and characterization of graphene and graphene oxide for supercapacitor applications, Ceram. Int. 49 (2023) 40–47, https://doi.org/10.1016/j.ceramint.2022.10.333.

[40] A.P.S. Raman, M. Aslam, C.Verma Naina, A. AlFantazi, P. Jain, A. Prajapat, P. Singh, K. Kumari, Composite nanoarchitectonics based on graphene oxide in energy storage and conversion: status, challenges & opportunities, J. Inorg. Organomet. Polym. (2024), https://doi.org/10.1007/s10904-024-03154-9.

[41] Y. Zhang, J. Wu, L. Jia, Y. Qu, Y. Yang, B. Jia, D.J. Moss, Graphene oxide for nonlinear integrated photonics laser, Photonics Rev. 17 (2023) 2200512, https://doi.org/10.1002/lpor.202200512.

[42] X. Xiao, Y. Zhang, L. Zhou, B. Li, Lin Gu, Photoluminescence and fluorescence quenching of graphene oxide: a review, Nanomaterials 12 (2022) 2444, https://doi.org/10.3390/nano12142444.

[43] N. Borane, R. Boddula, N. Odedara, J. Singh, M. Andhe, R. Patel, Comprehensive review on synthetic methods and functionalization of graphene oxide: emerging applications, Nano-Struct. Nano-Objects 39 (2024) 101282, https://doi.org/10.1016/j.nanoso.2024.101282.

[44] Y. Xie, M. Qi, X. Xiu, J. Yang, Y. Ren, Graphene oxide-based random access memory: from mechanism, optimization to application, J. Phys. D: Appl. Phys. 56 (2023) 033001, https://doi.org/10.1088/1361-6463/aca2b5.

[45] S. Singh, T.S.S.K. Naik, N. Shehata, L. Aguilar-Marcelino, K. Dhokne, S. Lonare, V. Chauhan, A. Kumar, J. Singh, P.C. Ramamurthy, A.H. Khan, N.A. Khan, M. H. Dehghani, Novel insights into graphene oxide-based adsorbents for remediation of hazardous pollutants from aqueous solutions: a comprehensive review, J. Mol. Liq. 369 (2023) 120821, https://doi.org/10.1016/j.molliq.2022.120821.

[46] O.J. Ajala, J.O. Tijani, M.T. Bankole, A.S. Abdulkareem, A critical review on graphene oxide nanostructured material: properties, Synthesis, characterization and application in water and wastewater treatment, Environ. Nanotechnol. Monit. Manage 18 (2022) 100673, https://doi.org/10.1016/j.enmm.2022.100673.

[47] M.I. Tayouri, S. Estaji, S.R. Mousavi, S.S. Khasraghi, R. Jahanmardi, S. Nouranian, M. Arjmand, H.Ali Khonakdar, Degradation of polymer nanocomposites filled with graphene oxide and reduced graphene oxide nanoparticles: a review of current status, Pol. Degrad. Stability 206 (2022) 110179, https://doi.org/10.1016/j.polymdegradstab.2022.110179.

[48] A. Razaq, F. Bibi, X. Zheng, R. Papadakis, S. Hassan M. Jafri, H. Li, Review on graphene-, graphene oxide-, reduced graphene oxide-based flexible composites: from fabrication to applications, Materials. (Basel) 15 (2022) 1012, https://doi.org/10.3390/ma15031012.

[49] J. Singh, N. Jindal, V. Kumar, K. Singh, Role of green chemistry in synthesis and modification of graphene oxide and its application: a review study, Chem. Phys. Impact 6 (2023) 100185, https://doi.org/10.1016/j.chphi.2023.100185.

[50] L. Guo, Z. Chen, H. Han, G. Liu, M. Luo, N. Cui, Hang Dong, Ming-Zheng Li, Advances and outlook in modified graphene oxide (GO)/epoxy composites for mechanical applications, Appl. Nanosci. 13 (2023) 3273–3287, https://doi.org/10.1007/s13204-022-02653-w.

[51] S. Sagadevan, Md Zillur Rahman 2, E. Léonard, D. Losic, Volker Hessel, Sensor to electronics applications of graphene oxide through AZO grafting, Nanomaterials 13 (2023) 846, https://doi.org/10.3390/nano13050846.

[52] Aminah N. Ghulam, Otávio A.L.dos Santos, Layla Hazeem, Bianca Pizzorno Backx, Mohamed Bououdina, Stefano Bellucci, Graphene Oxide (GO) materials—applications and toxicity on living organisms and environment, J. Funct. Biomater. 13 (2022) 77, https://doi.org/10.3390/jfb13020077.

[53] A. Anwar, T. Chang, C. Chen, Graphene oxide synthesis using a top–down approach and discrete characterization techniques: a holistic review, Carbon Lett. 32 (2022) 1–38, https://doi.org/10.1007/s42823-021-00272-z.

[54] M.D. Merchán, N. Pawar, A. Santamaria, R. Sanchez-Fernández, O. Konovalov, A. Maestro, M.Mercedes Velázquez, Structure of graphene oxide-phospholipid monolayers: a grazing incidence X-ray diffraction and neutron and X-ray reflectivity study, J. of Colloid and Inter. Sci. 655 (2024) 664–675, https://doi.org/10.1016/j.jcis.2023.11.022.
[55] B.S. Nugroho, Muh.Nur Khoiru Wihadi, Nakashima S, A.K. Amin, Oxidative debris on graphene oxide and its influence in the new route of formation for akaganeite (β-FeOOH) and maghemite (γ-Fe2O3) under mild condition, Carbon letters 34 (2024) 1329–1342, https://doi.org/10.1007/s42823-024-00692-7.
[56] M.G. Gonçalves, V.O. Costa, A.H.G. Martinez, B.M. Régnier, G.C.B. Gomes, A.J. G. Zarbin, E.S. Orth, Functionalization of graphene oxide via epoxide groups: a comprehensive review of synthetic routes and challenges, Front. Carbon 3 (2024) 1393077, https://doi.org/10.3389/frcrb.2024.1393077.
[57] Fang-Yu Zhan, Jian-Gang Guo, Xin-Ran Zhang, Xin-Liang Li, Adhesive forces between hydroxylated graphene and a single anisole: atomic force spectroscopy experiment and molecular dynamics simulation, Appl. Surf. Sci. 663 (2024) 160148, https://doi.org/10.1016/j.apsusc.2024.160148.
[58] S. Thakur, A. Bi, S. Mahmood, O.Ruzimuradov Samriti, R. Gupta, J. Cho, J. Prakash, Graphene oxide as an emerging sole adsorbent and photocatalyst: chemistry of synthesis and tailoring properties for removal of emerging contaminants, Chemosphere 352 (2024) 141483, https://doi.org/10.1016/j.chemosphere.2024.141483.
[59] Wenli Li, Huan Tang, Dan Zhang, T. Huang, B. Xing, Identifying the stripping of oxide debris from graphene oxide: evidence from experimental analysis and molecular simulation, Environ. Sci. Technol. 58 (2024) 5963–5973, https://doi.org/10.1021/acs.est.3c10044.
[60] L.S. Jairam, D. Shri M, A. Chandrashekar, T. Niranjana Prabhu, A. Arjun, H. B. Premkumar, Antibacterial and mechanical properties of cerium oxide nanoparticles modified glass ionomer cement, Mater. Chem. Phys. 315 (2024) 129040, https://doi.org/10.1016/j.matchemphys.2024.129040.
[61] E. Burresi, N. Taurisano, M.L. Protopapa, L. Latterini, M. Palmisano, L. Mirenghi, M. Schioppa, V. Morandi, R. Mazzaro, M. Penza, Influence of the synthesis conditions on the microstructural, compositional and morphological properties of graphene oxide sheets, Cer. Int. 46 (2020) 22067–22207, https://doi.org/10.1016/j.ceramint.2020.05.222.
[62] I. Rodriguez-Pastor, G. Ramos-Fernandez, H. Varela-Rizo, M. Terrones and I. Martin-Gullon, Towards the understanding of the graphene oxide structure: how to control the formation of humic- and fulvic-like oxidized debris Carbon 84 (2015) 299–309. https://doi.org/10.1016/j.carbon.2014.12.027.
[63] Q. Qiao, C. Liu, W. Gao, L. Huang, Graphene oxide model with desirable structural and chemical properties, Carbon. N. Y. 143 (2019) 566e577, https://doi.org/10.1016/j.carbon.2018.11.063.
[64] M.L. Protopapa, E. Burresi, M. Palmisano, E. Pesce, L. Latterini, N. Taurisano, G. Quaglia, R. Mazzaro, V. Morandi, Changing the microstructural and chemical properties of graphene oxide through a chemical route, Appl. Spectrosc. 76 (2022) 1452–1464, https://doi.org/10.1177/00037028221127048.
[65] Q. Lai, S. Zhu, X. Luo, M. Zou, et al., Ultraviolet–visible spectroscopy of graphene oxides, AIP. Adv. 2 (2012) 032146, https://doi.org/10.1063/1.4747817.
[66] L. Putria, B. Nga, K. Tanb, F. Sheng Limb, W. Ongc, W. Changb, S. Chaia, Tailoring the properties of oxygenated graphene with different oxidation degrees for noble-metal-free photocatalytic hydrogen evolution, Catal. Today 315 (2018) 93–102, https://doi.org/10.1016/j.cattod.2018.04.009.
[67] P. Chamoli1, M. Das, K. Kar, Structural, optical and electronic characteristics of N-doped graphene nanosheets synthesized using urea as reducing agent and nitrogen precursor, Mater. Res. Express 4 (2017) 015012, https://doi.org/10.1088/2053-1591/aa5776.
[68] J.P. Rourke, N.R. Wilson, Letter to the Editor: a defence of the two-component model of graphene oxide, Carbon. N. Y. 96 (2016) 339–340, https://doi.org/10.1016/j.carbon.2015.09.083.
[69] J.P. Rourke, P.A. Pandey, J.J. Moore, M. Bates, I.A. Kinloch, R.J. Young, Neil R. Wilson, The real graphene oxide revealed: stripping the oxidative debris from the graphene-like sheets, Angew. Chem. Int. Ed. 50 (2011) 3173–3177, https://doi.org/10.1002/anie.201007520.
[70] K. Ito, R. Saito, Daisuke Takimoto, S. Hideshima, W. Sugimoto, Electrochemical properties of debris free reduced graphene oxide synthesized from natural and synthetic graphite, Meet. Abstr. (2020), https://doi.org/10.1149/MA2020-02683519mtgabs. MA2020-02 3519.
[71] Z. Guo, S. Wang, G. Wang, Z. Niu, J. Yang, W. Wu, Effect of oxidation debris on spectroscopic and macroscopic properties of graphene oxide, Carbon. N. Y. 76 (2014) 203–211, https://doi.org/10.1016/j.carbon.2014.04.068.
[72] A.F. Faria, F. Perreault, M. Elimelech, Elucidating the role of oxidative debris in the antimicrobial properties of graphene oxide, ACS Appl. Nano Mater. 1 (2018) 1164–1174, https://doi.org/10.1021/acsanm.7b00332.
[73] A. Bonanni, A. Ambrosi, C.K. Chua, M. Pumeram, Oxidation debris in graphene oxide is responsible for its inherent electroactivity, ACS. Nano 8 (2014) 4197–4204, https://doi.org/10.1021/nn404255q.
[74] A.M. Dimiev, T.A. Polson, Contesting the two-component structural model of graphene oxide and reexamining the chemistry of graphene oxide in basic media, Carbon. N. Y. 93 (2015) 544–554, https://doi.org/10.1016/j.carbon.2015.05.058.
[75] A.M. Dimiev, L.B. Alemany, J.M. Tour, Graphene Oxide, Origin of acidity, its instability in water, and a new dynamic structural model, ACS. Nano 1 (2013) 576–588, https://doi.org/10.1021/nn3047378.
[76] T. Lee, S. Jiang, B.G. Alamani, J.P.R.P. Jucar, D.N.C. Potato, C. Chen, Environmentally benign and biocompatible sensing platform for electroanalytical determination of bisphenol A in the aquatic environment 28 (2022) 100713. https://doi.org/10.1016/j.scp.2022.100713.
[77] J. Zhang, C. Xiong, Y. Li, H. Tang, X. Meng, W. Zhu, The critical contribution of oxidation debris on the acidic properties of graphene oxide in an aqueous solution, J. of Hazar. Mater. 402 (2021) 123552, https://doi.org/10.1016/j.jhazmat.2020.123552.
[78] O. Yu. Posudievsky, O.A. Khazieieva, O.A. Kozarenko, G.I. Dovbeshko, V. G. Koshechko, V.D. Pokhodenko, Effect of the mechanochemical preparation on the fractional composition and spectral characteristics of graphene oxide, Theor. and Exper. Chemistry 53 (2017) 93–99, https://doi.org/10.1007/s11237-017-9504-z.
[79] C. Hu, Y. Liu, Y. Yang, J. Cui, Z. Huang, Y. Wang, L. Yang, H. Wang, Y. Xiao, J. Rong, One-step preparation of nitrogen-doped graphene quantum dots from oxidized debris of graphene oxide, J. Mater. Chem. B 1 (2013) 39–42.
[80] W. Li, H. Tang, D. Zhang, T. Huang, B. Xing, Identifying the stripping of oxide debris from graphene oxide: evidence from experimental analysis and molecular simulation, Environ. Sci. Technol. 58 (2024) 5963–5973, https://doi.org/10.1021/acs.est.3c10044.
[81] K. Lee, W. Cheng, C. Chen, J. Shyue, C. Nieh, C. Chou, J. Lee, Y. Lee, C. Cheng, S. Y. Chang, T.C. Yang, M. Cheng, B. Lin, Excitation-dependent visible fluorescence in decameric nanoparticles with monoacylglycerol cluster chromophores, Nat. Commun. 4 (2013) 1544, https://doi.org/10.1038/ncomms2563.
[82] M.J. Krysmann, A. Kelarakis, P. Dallas, E.P. Giannelis, Formation mechanism of carbogenic nanoparticles with dual photoluminescence emission, J. Am. Chem. Soc. 134 (2012) 747–750, https://doi.org/10.1021/ja204661r.
[83] A.M. Laera, G. Cassano, E. Burresi, M.L. Protopapa, Michele Penza, A graphene oxide flexible sensor for humidity detection, Eng. Proc. 48 (2023) 4, https://doi.org/10.3390/CSAC2023-14884.4.
[84] A.U. Baes, P.R. Bloom, Fulvic Acid Ultraviolet-Visible Spectra: influence of Solvent and pH, Soil Sci. Soc. Am. J. 54 (1990) 1248–1254, https://doi.org/10.2136/sssaj1990.03615995005400050008x.
[85] Yu Lim Hong, Jieon Lee, Bon-Cheol Ku, Kyungtae Kang, Seunghyun Lee, Seongwoo Ryub, Young-Kwan Kima, The influence of oxidative debris on fragmentation laser desorption/ionization process of graphene oxide derivatives, New J. Chem. 42 (2018) 12692–12697, https://doi.org/10.1039/x0xx00000x.
[86] N. Jiang, D. Zhu, Z. Su, M.R. Bryce, Recent advances in oligomers/polymers with unconventional chromophores, J. Mater. Chem. Front. 5 (2021) 60–75, https://doi.org/10.1039/d0qm00626b.
[87] R. Bresoli-Obach, J.A. Castro-Osma, S. Nonell, A. Lara-Sanchez, C. Martin, Polymers showing cluster triggered emission as potential materials in biophotonic applications, J. Phot. & Photob. Rev. 58 (2024) 100653, https://doi.org/10.1016/j.jphotochemrev.2024.100653.
[88] R. Deams, J. Kim, M.R. Machacck, T.M. Swager, A Poly(p-phenyleneethynylene) with Highly Emissive Aggregated Phase, J. Am. Chem. Soc. 122 (2000) 8565–8566.
[89] J. Luo, Z. Xie, J.W.Y. Lam, L. Cheng, H. Chen, C. Qiu, H.S. Kwok, X. Zhan, Y. Liu, D. Zhu, B.Z. Tang, Aggregation-induced emission of 1-methyl-1,2,3,4,5-Pentaphenylsilole, Chem. Commun. (2001) 1740–1741, https://doi.org/10.1039/b105159h.
[90] D. Wang, T. Imae, Fluorescence Emission from Densdrimers and its pH dependence, J. Am. Chem. Soc. 126 (2004) 13204–13205, https://doi.org/10.1021/ja0454992.
[91] Z. Wang, H. Zhang, S. Li, D. Lei, B.Z. Tang, R. Ye, Recent advances in clusterluminescence topics, Curr. Chem. 379 (2021) 1–22, https://doi.org/10.1007/978-3-030-89933-2_2.
[92] M. Levitus, K. Schmieder, H. Ricks, K.D. Shimizu, U.H.F. Bunz, M.A. Garcia-Garibay, Steps to demarcate the effects of chromophore aggregation and planarization in poly(phenyleneethynylene)s. 1. Rotationally interrupted conjugation in the excited states of 1,4-bis(phenylethynyl)benzene, J. Am. Chem. Soc. 123 (2001) 4259–4265, https://doi.org/10.1021/ja003959v.
[93] J. Guan, C. Shen, J. Peng, J. Zheng, What Leads to Aggregation-Induced Emission? J. Phys. Chem. Lett. 12 (2021) 4218–4226, https://doi.org/10.1021/acs.jpclett.0c03861.